



Cite this: *Chem. Commun.*, 2025, 61, 16970

Received 17th June 2025,
Accepted 22nd September 2025

DOI: 10.1039/d5cc03419a

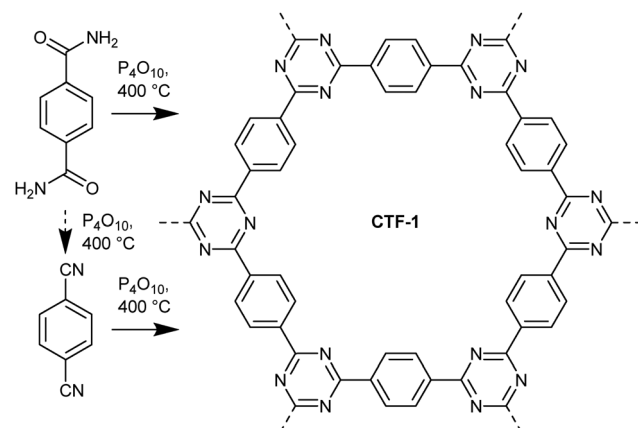
rsc.li/chemcomm

Polycondensation of various aromatic amides in P_4O_{10} at 400 °C yields covalent triazine frameworks intergrown with a polyphosphoric acid framework (POF-CTFs). Compared to ionothermal analogs, they feature a shorter reaction time and strongly increased framework polarity for water and SO_2 uptake, and SO_2/CO_2 selectivity.

Covalent triazine frameworks, CTFs, a subclass of porous organic polymers, are represented by idealized periodic networks, featuring three-connected 1,3,5-triazine units as nodes which together with typical linear connectors assemble into planar sheets of hexagonal net topology (Scheme 1).

The large surface areas, hydrothermal stabilities and nitrogen-rich structures afford CTFs with promising properties for, *e.g.*, gas adsorption, pollutant removal and catalysis, filler in mixed-matrix membranes, supports for metal nanoparticles.^{1–5}

The typical synthesis of CTFs, as described by Kuhn *et al.*, employs a $ZnCl_2$ -mediated ionothermal polymerization process, whereby di-nitrile monomers undergo trimerization at temperatures above 400 °C.^{6,7} The most important alternative synthesis to CTFs uses Brønsted superacids such as trifluoromethanesulfonic acid to enable the polymerization of nitriles at lower temperatures.^{8,9} Another alternative is the Friedel–Crafts polymerization, in which cyanuric chloride is reacted with aromatic molecules in the presence of anhydrous $AlCl_3$.¹⁰ All these methods have significant drawbacks. Ionothermal polymerization requires high temperatures, causing carbonization with loss of nitrogen, which intensifies with the increase in temperature, and while the surface area also grows, the loss of nitrogen renders those materials closer to active carbons and



Scheme 1 The P_4O_{10} -mediated reactions, equivalent to polycondensation of 1,4-benzene dicarboxamide (terephthalamide) into (idealized) CTF-1.

leaves hard-to-remove $ZnCl_2$ metal impurities from the needed 5–10 times molar excess.^{2,7} The superacid approach typically leads to CTFs of low porosity and faces industrial hurdles due to the corrosive nature, significant price and scalability issues.^{2,11} The Friedel–Crafts route suffers from poor economic and environmental viability.² Yu *et al.* reported a synthesis strategy for CTFs, utilizing ‘phosphorus pentoxide’ (P_4O_{10}).¹² This approach relies on the polycondensation of aromatic primary amide groups to form 1,3,5-triazine rings (Scheme 1).

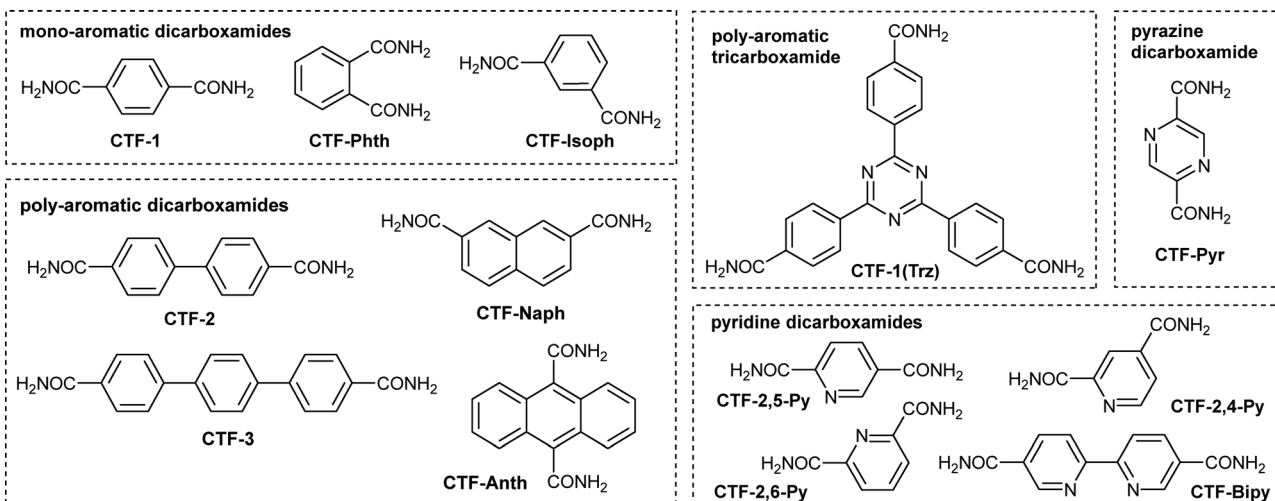
It was stated that CTF-1 and CTF-2 (from biphenyl-4,4'-dicarboxamide) through the P_4O_{10} route exhibited a high crystallinity and a large specific surface area,^{12,13} when compared to the ionothermally synthesized CTF analogs.⁴ The P_4O_{10} method is also more environmentally friendly compared to the large scale uses of metal salts or superacids. However, the P_4O_{10} -based approach has only been reported for two CTFs and is not investigated regarding the scope of dicarboxamide reactants, the nitrogen content, and possible gains from the presence of phosphorus oxygen species in the CTF. P_4O_{10} is

^a Institut für Anorganische Chemie und Strukturchemie, Heinrich-Heine-Universität, 40204 Düsseldorf, Germany. E-mail: janik@uni-duesseldorf.de

^b Solid-State NMR Laboratory, Bundesanstalt für Materialforschung und -prüfung (BAM), Richard-Willstätter-Str. 11, 12489, Berlin, Germany

^c Institut für Nichtklassische Chemie e. V., Permoserstraße 15, 04318 Leipzig, Germany





Scheme 2 Carboxamide monomers used in this work for the P_4O_{10} -mediated synthesis of CTFs with the CTF acronym given below the monomer formula.

known to generate a three-dimensional network corner-sharing PO_4 tetrahedra.¹⁴ In the context of the CTF synthesis, the ability of forming polymeric structures renders P_4O_{10} a porogen with a potentially strong templating effect on the formation of the CTF frameworks. We first attempted to remove the phosphate species by thorough washing procedures (Section S3) but we realized that the CTFs retained a large phosphate content as an integral part of the material and that we reproducibly obtained polyphosphoric acid-CTF composites which we subsequently analyzed. The formed material could be viewed as consisting of two intermingled, interpenetrated or intergrown frameworks.

An interesting test field for CTFs with less carbonization, *i.e.* higher polar nitrogen content and hydrophilic polyphosphoric acid, is water sorption for heat transformation^{15,16} or water harvesting.^{17–22} This study aims to advance the P_4O_{10} -mediated synthesis of CTFs focusing on the influence of the amide monomer on the resultant adsorbent properties (Scheme 2).

The CTFs from various dicarboxamide monomers and one tricarboxamide monomer, synthesized *via* the P_4O_{10} route, were obtained after 24 h of reaction time as black solids with a glass-like morphology, which yielded fine black powders after washing (see Section S3). The FT-IR spectra (Fig. S1a) confirmed triazine formation by C=N stretching vibrations bands around 1515 cm^{-1} and 1360 cm^{-1} ,²³ and the absence of the $\delta(N-H)$ amide band at 1650 cm^{-1} ,²⁴ which confirms full conversion of the monomers. Bands in the $1000\text{--}1200\text{ cm}^{-1}$ range, (P=O symmetric, P–O–C and P–O–P asymmetric stretchings), along with a peak at $\sim 1250\text{ cm}^{-1}$ (P–O–H bending) are attributed to phosphate functionalities.²⁵ Scanning electron microscopy (SEM) shows the typical shard-like morphology (Fig. S8–S15). Solid-state 1H , ^{13}C , ^{31}P NMR with 1H – ^{31}P cross-polarization (CP), ^{31}P – 1H HETCOR and reverse CP experiments verify the formation of triazine ring and the inclusion of phosphate species in the pores (see Section S6 for details). XPS on CTF-1 and CTF-Bipy to confirmed the presence of phosphorus in the CTF composites (see Section S9 for details).

The elemental composition of CTFs with a phosphorus–oxygen framework (POF-CTFs) was assessed by CHN combustion and SEM-EDX (Tables S3 and S4). CHN analysis confirmed successful CTF formation, with C/N ratios indicating higher nitrogen retention and lower carbonization in the P_4O_{10} -derived CTF-1 compared to the ionothermal CTF-1(400)– $ZnCl_2$.²⁶ As also observed by Yu *et al.*, CHN analysis revealed a residual mass which was identified by EDX as phosphorus and oxygen, consistent with a polyphosphoric acid network.¹² In TGA the onset of the evident disintegration of the CTFs starts at approx. $450\text{ }^\circ\text{C}$ in all cases (Fig. S18).

Nitrogen sorption isotherms (Fig. 1 and Fig. S19) reveal predominantly microporous structures (Type I/Ib), with minor meso- or macroporosity (Type II). In contrast, mono-pyridine and pyrazine CTFs show Type III behavior and negligible surface area (Fig. S13) and were excluded from further analysis. BET surface areas range from $440\text{ m}^2\text{ g}^{-1}$ (CTF-Isoph) to

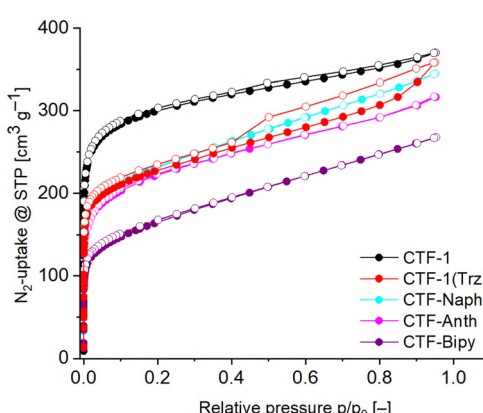


Fig. 1 N_2 -adsorption isotherms (77 K) for selected POF-CTFs which were also studied for water, SO_2 and CO_2 sorption (filled symbols adsorption, empty symbols desorption). For the isotherms of other CTFs see Fig. S19.



1460 m² g⁻¹ (CTF-2), with the highest values observed for the linear linkers (CTF-1, -2, -3). In contrast, the non-linear, bent or bulkier linkers show lower surface areas (Table S5). The *meta*-branched CTF-Isoph (440 m² g⁻¹) and the *ortho*-branched CTF-Phth (690 m² g⁻¹) feature approximately half of the CTF-1 surface area. Pore volumes of the POF-CTFs span 0.30–0.77 cm³ g⁻¹, and the pore size distribution (Fig. S21) confirms dominant microporosity (\sim 0.5–2 nm), with minor mesopore contributions up to \sim 5 nm. A hierachic porosity with mesopore contributions is a positive prerequisite for applications. This could be viewed as an indirect confirmation that the continuous random network arising from P₄O₁₀ acts as an efficient porogen also at the mesoporous level.

CTF-1(Trz), derived from the pre-trimerized building block, tris(*p*-carbamoylphenyl)triazine (Scheme 2), gives a lower BET surface area compared to CTF-1 (830 m² g⁻¹ vs. 1150 m² g⁻¹), although the use of the pre-trimerized building block could have been expected to yield the idealized structure with higher probability than the smaller CTF-1 building block.

The incorporation of pyridine and pyrazine moieties to the structure of the CTFs aimed to increase the number of nitrogen sites. Unfortunately, the use of any type of monomer containing at least one amide group in the *ortho*-position relative to the N-atom of the ring led to failure, *i.e.*, no microporous- or even mesoporous materials were obtained (Fig. S20). We suggest the involvement of amidophosphate (or similar, P–N bond containing) bridges for which the *ortho*-situated N atom increases the susceptibility towards nucleophilic attack, leading to collapse of the material during work-up, upon contact with a solution containing phosphoric acids. However, in the case of (2,2'-bipyridine)-4,4'-dicarboxamide, where the amide resides only at the *meta*-positions, the synthesis was moderately successful regarding the surface area (600 m² g⁻¹).

Despite the high stability of CTFs, water vapor adsorption remains underexplored, as their typically hydrophobic nature resulting from low nitrogen and high carbon content typically limits water uptake to the high relative pressure region.^{20,27,28} However, previous studies have demonstrated that the incorporation of polar functional groups or heteroatoms in the CTF framework can enhance hydrophilicity.²⁰ Comparing the POF-CTF-1 with the ionothermal ZnCl₂-derived CTF-1(400) (without P₄O₁₀) shows both the higher and earlier water uptake (Fig. 2). Polyphosphoric acids exhibit particularly strong hydrophilic character, making the POF-CTFs especially attractive for improving water adsorption performance. The water sorption isotherms (Fig. 2) show that more than 50% of the total water uptake occurs at relative pressures of less than 0.5 (50% relative humidity). The steep water uptake at pressures below $p/p_0 \approx 0.3$ is due to adsorption at polar phosphorus–oxygen sites. The subsequent gradual uptake up to $p/p_0 \approx 1.0$ reflects secondary multilayer adsorption and cluster formation. The pronounced hysteresis points to capillary condensation and delayed desorption. Notably, the low-pressure uptake is significantly higher than in other reported CTFs: pym-CTF500 reaches 115 cm³ g⁻¹ at $p/p_0 = 0.1$,²⁰ the POF-CTF-1 achieves 145 cm³ g⁻¹. The ionothermally (ZnCl₂) obtained CTF-Bipy achieves only

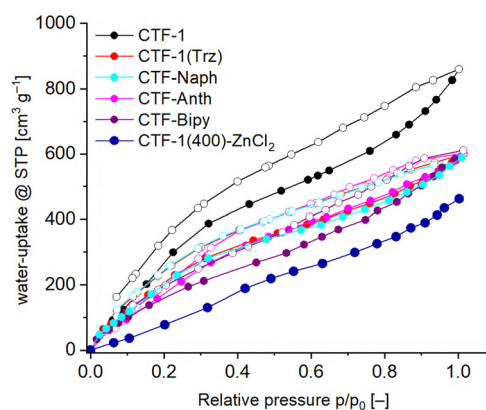


Fig. 2 Water sorption isotherms of selected POF-CTFs at 293 K and of CTF-1(400)-ZnCl₂ (no P₄O₁₀) (re-synthesized and measured) (filled symbols adsorption, empty symbols desorption). See Fig. S22 for the water uptake as mmol g⁻¹ and g g⁻¹.

\sim 50 cm³ g⁻¹,²⁰ while POF-CTF-Bipy adsorbs \sim 100 cm³ g⁻¹, which is nearly twice as much, with a similar BET area.

Polar porous materials with low-pressure selective SO₂ uptake are of interest for the capture and sensing of this gas.²⁹ The SO₂ adsorption isotherms (Fig. 3) show a steep initial uptake at low pressures (up to 0.1 bar), followed by a gradual increase without fully reaching saturation at 1 bar and 293 K. The initial steep increase reflects the filling of the micropores.

The desorption branches have a wide hysteresis, which closes only at low pressure. The protracted character of the loops signals a broad distribution of pore sizes with a fraction exhibiting ink-bottle-type morphologies. At pressures below 0.1 bar, CTF-1 exhibits the highest absolute SO₂ uptake, surpassing that of the reported ionothermally synthesized CTF-1(400)-ZnCl₂ and CTF-1(600)-ZnCl₂,²⁶ followed by CTF-Naph, CTF-Anth, CTF-3, CTF-Bipy, and CTF-1(Trz) with comparable performance. In contrast, CTF-Phth, CTF-2, and CTF-Isoph show significantly lower uptakes (Fig. S17).

The character of the CO₂ adsorption isotherms is clearly different with regard of the steep initial uptake observed for SO₂. CO₂ features are more gradual uptake in the low-pressure range, and the total uptake at 1 bar is less than a third of the SO₂ amount. Furthermore, the hysteresis observed for CO₂ is far less pronounced than in the case of SO₂. These observations indicate the expected higher affinity of the CTF materials toward SO₂ compared to CO₂. In addition, breakthrough experiments were performed, which further confirm the preferential sorption of SO₂ over CO₂ (Section S14.3). An immediate elution of N₂ and CO₂ was observed for both CTF-1 and CTF-Bipy, whereas SO₂ exhibited pronounced retention. For CTF-1 (Fig. S32), the SO₂ retention time, normalized to adsorbent mass, was \approx 83 min g⁻¹, while CTF-Bipy (Fig. S35) displayed a substantially longer retention of \approx 138 min g⁻¹. These results demonstrate that CTF-Bipy possesses the highest SO₂ affinity, corroborating the IAST calculations (Section S14.4), and highlight the role of the higher nitrogen content in enhancing SO₂ adsorption capacity.

The P₄O₁₀-mediated method of CTF synthesis starting from amides was successfully employed for a wide series of

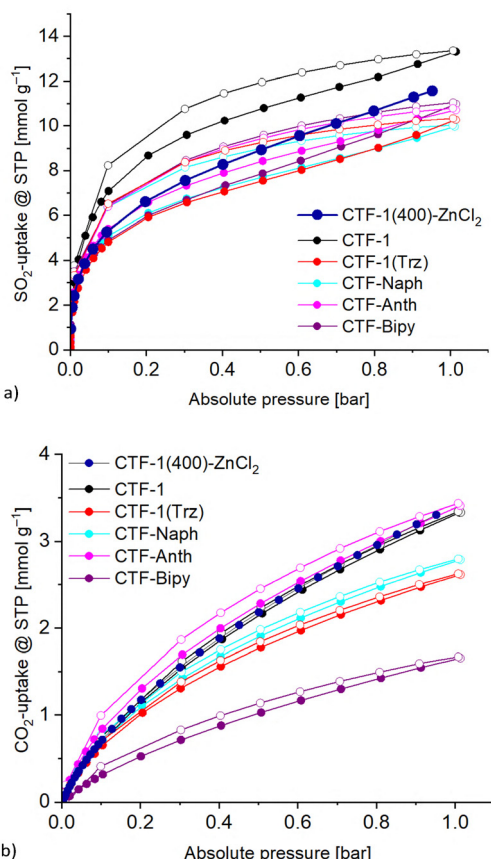


Fig. 3 Adsorption–desorption isotherms (293 K) for selected CTFs up to 1 bar: (a) SO₂ and (b) CO₂ (filled symbols adsorption, empty symbols desorption). For the isotherms of other CTFs see Fig. S23. The expansion of the adsorption isotherms in the pressure range below 0.1 bar is shown in Fig. S24, the capacities at selected pressures (0.01, 0.05, and 0.1 bar) are summarized in Table S6. The data for CTF-1(400)-ZnCl₂ is from ref. 26. For SO₂ adsorption over five cycles see Section S14.2.

non-functionalized aromatic amide substrates with phenyl, biphenyl, bipyridyl, terphenyl, naphthyl, anthracenyl or tri(phenyl)triazine cores. A failure or limitation of the method is noted for nitrogen-functionalized aromatic cores such as pyridine and pyrazine. Compared to the traditional ZnCl₂-based ionothermal method using nitriles, a metal-free CTF with intergrown polar polyphosphoric acid residues was obtained which exhibit higher uptakes of the polar adsorbates H₂O and SO₂ as well as improved low pressure SO₂/CO₂ selectivities.

Support by the Interdisciplinary Centre for Analytics on the Nanoscale of the University of Duisburg for XPS analysis and by the DAAD (project 57724286) are gratefully acknowledged.

Conflicts of interest

There are no conflicts to declare.

Data availability

The data supporting this article have been included as part of the supplementary information (SI). Supplementary information: synthesis, methods, IR, ss-NMR, PXRD, SEM-EDX, XPS, elemental analysis, TGA, gas sorption with breakthrough experiments. See DOI: <https://doi.org/10.1039/d5cc03419a>.

Notes and references

- 1 L. Liao, M. Li, Y. Yin, J. Chen, Q. Zhong, R. Du, S. Liu, Y. He, W. Fu and F. Zeng, *ACS Omega*, 2023, **8**, 4527–4542.
- 2 M. Liu, L. Guo, S. Jin and B. Tan, *J. Mater. Chem. A*, 2019, **7**, 5153–5172.
- 3 J.-S. M. Lee and A. I. Cooper, *Chem. Rev.*, 2020, **120**, 2171–2214.
- 4 C. Krishnaraj, H. S. Jena, K. Leus and P. van der Voort, *Green Chem.*, 2020, **22**, 1038–1071.
- 5 S. Aggarwal and S. K. Awasthi, *Dalton Trans.*, 2024, **53**, 11601–11643.
- 6 P. Kuhn, A. Forget, D. Su, A. Thomas and M. Antonietti, *J. Am. Chem. Soc.*, 2008, **130**, 13333–13337.
- 7 P. Kuhn, M. Antonietti and A. Thomas, *Angew. Chem., Int. Ed.*, 2008, **47**, 3450–3453.
- 8 X. Zhu, C. Tian, S. M. Mahurin, S.-H. Chai, C. Wang, S. Brown, G. M. Veith, H. Luo, H. Liu and S. Dai, *J. Am. Chem. Soc.*, 2012, **134**, 10478–10484.
- 9 S. Ren, M. J. Bojdys, R. Dawson, A. Laybourn, Y. Z. Khimyak, D. J. Adams and A. I. Cooper, *Adv. Mater.*, 2012, **24**, 2357–2361.
- 10 H. Lim, M. C. Cha and J. Y. Chang, *Macromol. Chem. Phys.*, 2012, **213**, 1385–1390.
- 11 R. Sun and B. Tan, *Chem. – Eur. J.*, 2023, **29**, e202203077.
- 12 S. Y. Yu, J. Mahmood, H. J. Noh, J. M. Seo, S. M. Jung, S. H. Shin, Y. K. Im, I. Y. Jeon and J. B. Baek, *Angew. Chem., Int. Ed.*, 2018, **57**, 8438–8442.
- 13 S.-Y. Yu, J. C. Kim, H.-J. Noh, Y.-K. Im, J. Mahmood, I.-Y. Jeon, S. K. Kwak and J.-B. Baek, *Cell Rep. Phys. Sci.*, 2021, **2**, 100653.
- 14 W. H. Zachariasen, *J. Am. Chem. Soc.*, 1932, **54**, 3841.
- 15 D. M. Steinert, S.-J. Ernst, S. K. Henninger and C. Janiak, *Eur. J. Inorg. Chem.*, 2020, 4502–4515.
- 16 E. Hastürk, S.-J. Ernst and C. Janiak, *Curr. Opin. Chem. Eng.*, 2019, **24**, 26–36.
- 17 W. Xu and O. M. Yaghi, *ACS Cent. Sci.*, 2020, **6**, 1348–1354.
- 18 K. Park, K. Lee, H. Kim, V. Ganesan, K. Cho, S. K. Jeong and S. Yoon, *J. Mater. Chem. A*, 2017, **5**, 8576–8582.
- 19 Y. Byun, S. H. Je, S. N. Talapaneni and A. Coskun, *Chem. – Eur. J.*, 2019, **25**, 10262–10283.
- 20 S. Hug, L. Stegbauer, H. Oh, M. Hirscher and B. V. Lotsch, *Chem. Mater.*, 2015, **27**, 8001–8010.
- 21 H. Mabuchi, T. Irie, J. Sakai, S. Das and Y. Negishi, *Chem. – Eur. J.*, 2024, **30**, e202303474.
- 22 C. Sun, D. Sheng, B. Wang and X. Feng, *Angew. Chem., Int. Ed.*, 2023, **62**, e202303378.
- 23 W. Zhang, C. Li, Y.-P. Yuan, L.-G. Qiu, A.-J. Xie, Y.-H. Shen and J.-F. Zhu, *J. Mater. Chem.*, 2010, **20**, 6413–6415.
- 24 A. Mohabbat, I. Boldog, T. H. H. Sohi, N. Reistel, P. Seiffert and C. Janiak, *Crystals*, 2025, **15**, 406.
- 25 C. Sun and D. Xue, *CrystEngComm*, 2013, **15**, 10445–10450.
- 26 P. Brandt, A. Nuhnen, S. Öztürk, G. Kurt, J. Liang and C. Janiak, *Adv. Sustainable Syst.*, 2021, **5**, 2000285.
- 27 S. Dey, A. Bhunia, H. Breitzke, P. B. Groszewicz, G. Buntkowsky and C. Janiak, *J. Mater. Chem. A*, 2017, **5**, 3609–3620.
- 28 S. Dey, A. Bhunia, I. Boldog and C. Janiak, *Microporous Mesoporous Mater.*, 2017, **241**, 303–315.
- 29 W. Zhao, J. L. Obeso, V. B. López-Cervantes, M. Bahri, E. Sánchez-González, Y. A. Amador-Sánchez, J. Ren, N. D. Browning, R. A. Peralta, G. Barcaro, S. Monti, D. Solis-Ibarra, I. A. Ibarra and D. Zhao, *Angew. Chem., Int. Ed.*, 2025, **64**, e202415088.

